



**Fermi National Accelerator Laboratory**

**FERMILAB-Conf-87/62**  
2563.000

## **CDF Calorimetry\***

**H.B. Jensen**  
Fermi National Accelerator Laboratory  
P.O. Box 500, Batavia, Illinois 60510

March 1987

\*Invited talk presented at the International Conference on Advances in Experimental Methods for Colliding Beam Physics, Stanford Linear Accelerator Center, Stanford, CA, March 9-13, 1987.



Operated by Universities Research Association Inc. under contract with the United States Department of Energy

# CDF CALORIMETRY

CDF Collaboration\*

Presented by Hans B. Jensen  
Fermi National Accelerator Laboratory\*  
P.O. Box 500, Batavia, Illinois 60510, U.S.A.

## Abstract

The Collider Detector at Fermilab (CDF) is a large detector built to study 2 TeV  $\bar{p}p$  collisions at the Fermilab Tevatron. The calorimetry, which has polar angle coverage from  $2^\circ$  to  $178^\circ$ , and complete azimuthal coverage within this region, forms the subject of this paper. It consists of both electromagnetic shower counters (EM calorimeters) and hadron calorimeters, and is segmented into about 5000 "towers" or solid angle elements.

## 1. Introduction

During a short test run in October of 1985, parts of the CDF detector were used to record the first  $\bar{p}p$  collisions in the Fermilab Tevatron. Detector installation was completed towards the end of 1986, and a first data taking period with 1.8 TeV collisions is now in progress.

The CDF collaboration is international, with members from universities and laboratories in the U.S., Italy and Japan. A list of the collaboration is given in Appendix 1.

Calorimetry plays an important role in a detector such as CDF, because it provides the basic information in the detection of quark- and gluon jets. It also gives a good measurement of the energy of electrons, and, in some cases, an indirect measurement of neutrino momentum.

There are, altogether, seven calorimeter systems in the detector: central EM calorimeters [1], central hadron calorimeters [2], endwall hadron calorimeters [2], endplug EM calorimeters [3], endplug hadron calorimeters [4], forward EM calorimeters [5] and forward hadron calorimeters [6].

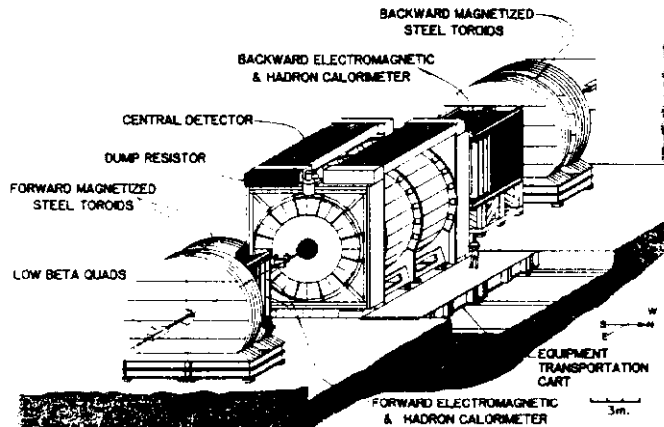


Fig. 1 Isometric drawing of CDF

\*The collaboration is listed in Appendix 1.  
\*Operated by Universities Research Association, Inc., under contract with the U.S. Department of Energy

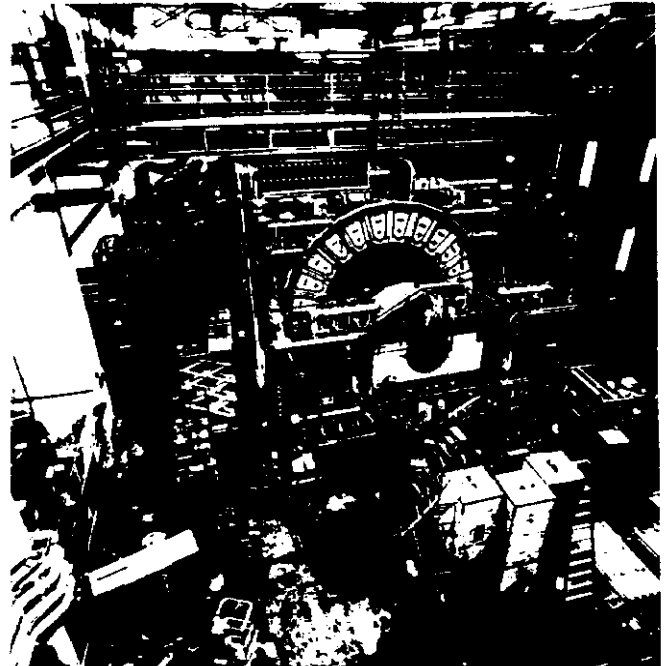


Fig. 2 Photograph of the central detector. The central, endwall and endplug calorimeters are clearly seen. The central and endplug calorimeters are in the positions used for cabling

## 2. General properties

The detector consists of a central detector and symmetrical forward-backward detectors, see Fig. 1. A photograph of the central detector is shown in Fig. 2. The location of the calorimeters with respect to the interaction region, which is at the center of the detector, can be seen in Fig. 3. The 48 "wedge" modules of central calorimetry (EM and hadron) form four C-shaped "arches" around the 3 m diameter, 5 m long, 1.5 Tesla solenoid coil. The endplug EM calorimeters are located in the essentially uniform solenoidal field. The steel plates of the endplug and endwall hadron calorimeters form part of the solenoid flux return path. The forward calorimeters are in a field-free region. The minimum distance from the center of the detector to the front faces of both central and endplug calorimeters is 173 cm, while the distance to the forward calorimeters is 618 cm.

Charged particle tracking systems are located between the interaction region and the calorimeters. The momentum resolution in the field of the solenoid is  $\Delta p_T/p_T = 0.2\% \cdot p_T$  (in GeV/c) for polar angles larger than  $40^\circ$  to the beams, but deteriorates at smaller polar angles. For a description of the full detector, see [7].

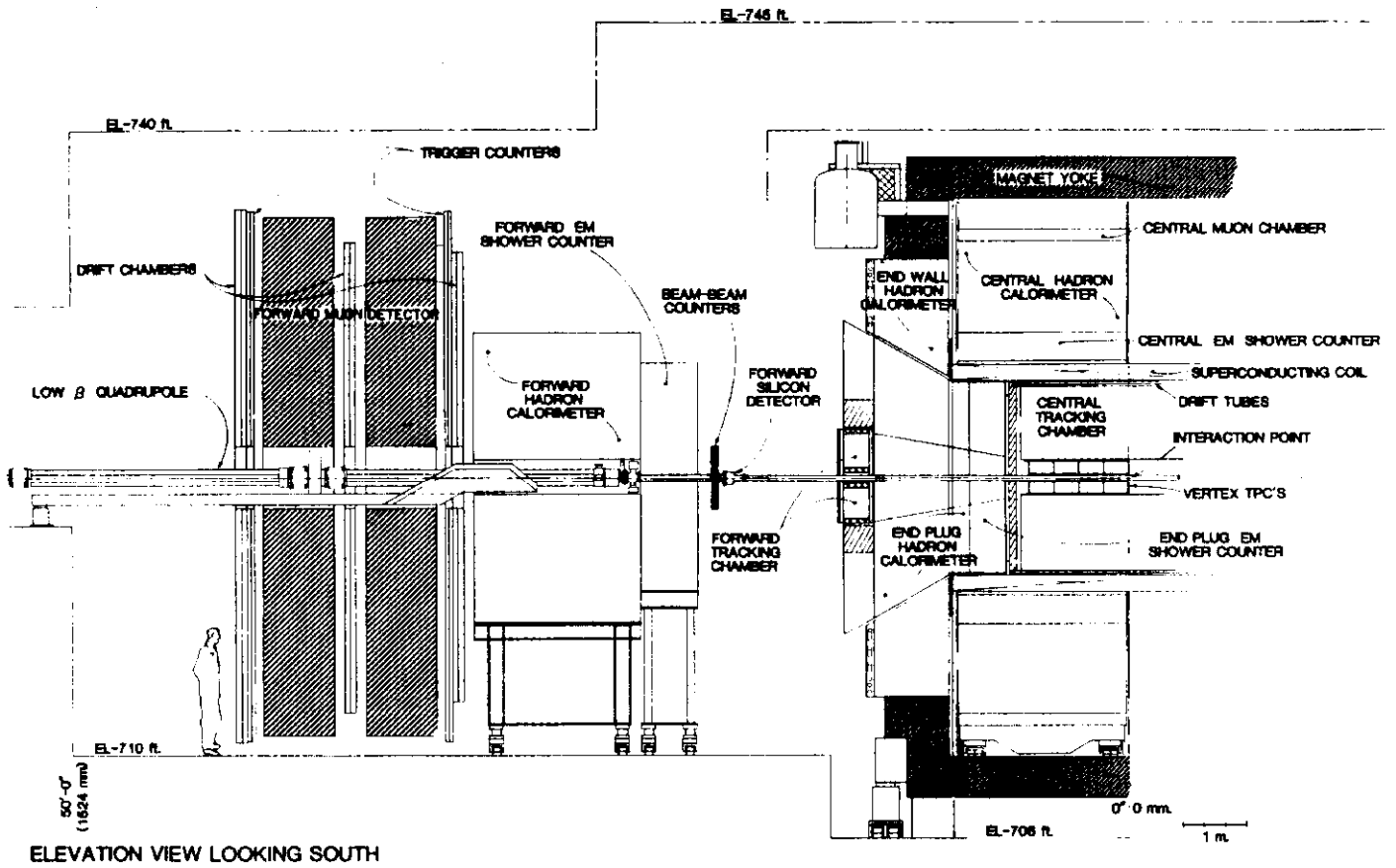


Fig. 3 A cut through one half of CDF

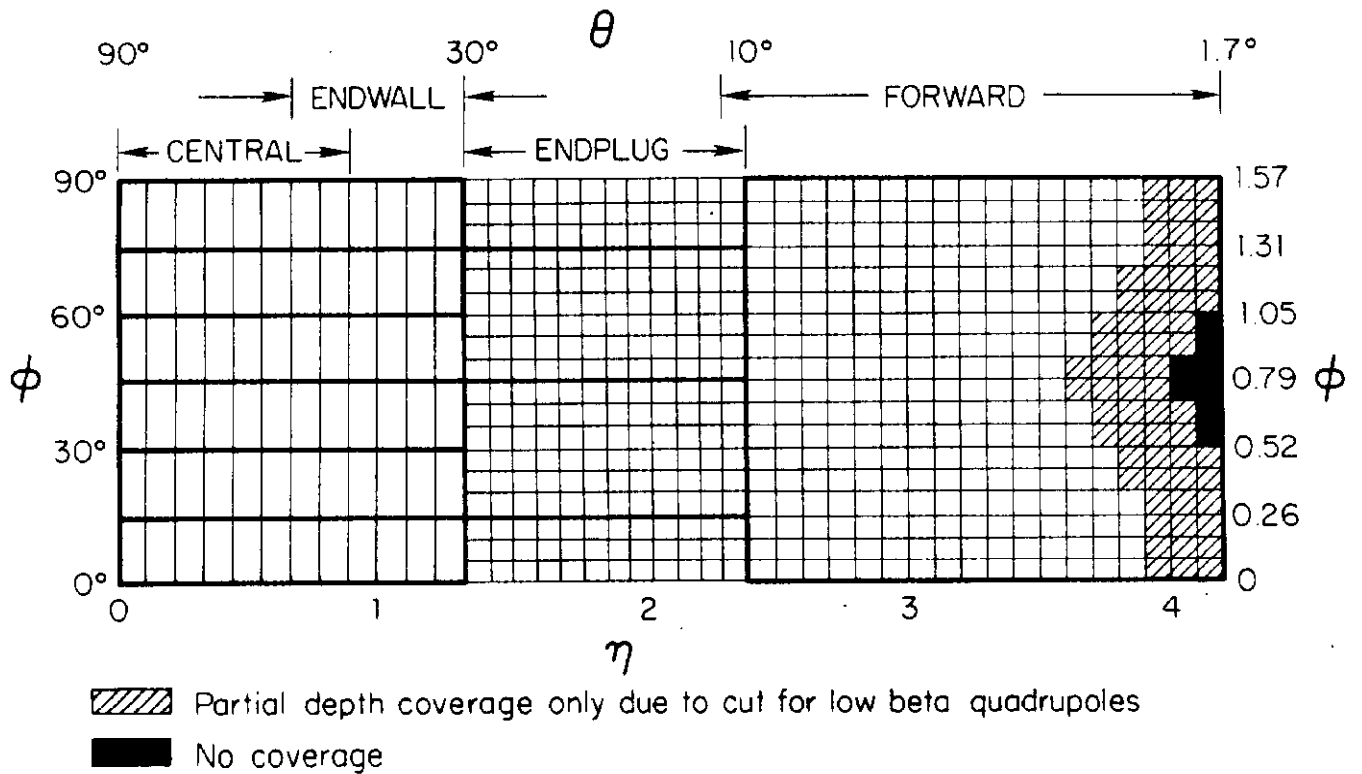


Fig. 4 One quadrant of hadron calorimeter towers. The heavy lines indicate module or chamber boundaries. The EM calorimeters have complete  $\phi$ -coverage out to  $\eta = 4.2$ .

The calorimeters are all of the sampling type. The EM calorimeters contain lead as the absorber, whereas the hadron calorimeters have steel plates. The active medium is scintillator in the region of large polar angles,  $\theta$ , to the beams (central and endwall calorimeters), and proportional tube chambers with cathode pad readout at small angles to the beams (endplug and forward calorimeters). A summary of calorimeter properties is given in Table 1. Note that typical calorimeter signals are, by design, quite similar for all the calorimeter systems.

The angular coverage of the calorimeters is  $2\pi$  in the azimuthal angle  $\phi$ , and from  $-4.2$  to  $+4.2$  in pseudorapidity  $\eta$ , which is defined as  $-\ln \tan(\theta/2)$ , except that the forward hadron calorimeter in the interval  $3.6 < \eta < 4.2$  (and  $-4.2 < \eta < -3.6$ ) has incomplete  $\phi$ -coverage. Expressed in  $\theta$ , the coverage is  $2^\circ < \theta < 178^\circ$ .

The calorimeters are all subdivided into many cells. Each cell is a matching "tower" or solid angle element of EM and hadron calorimeter. Such a geometry facilitates the reconstruction of energy patterns in the detector for physics analysis. The calorimeter tower segmentation can be represented as rectangles in the  $\eta$ - $\phi$  plane. The tower size is given by  $\Delta \eta \Delta \phi = 0.1 \times 0.09$  (approximately) for the pad readout of the proportional tube chambers, while  $\Delta \eta \Delta \phi = 0.1 \times 0.26$  (approximately) for the scintillator calorimeters. The density of particles in typical inelastic collisions is more or less uniform in  $\eta$ - $\phi$  space. Fig. 4 shows the grid of hadron calorimeter towers in one quadrant of the detector, together with module or chamber boundaries. In the endplug EM calorimeter, the chambers cover  $90^\circ$  in  $\phi$ , but the grid of EM calorimeter towers is otherwise essentially the same as that shown in Fig. 4. The boundaries between calorimeter systems are at  $\theta = 10^\circ$  (endplug - forward),  $\theta = 30^\circ$  (endplug hadron calorimeter - endwall hadron calorimeter) and  $\theta = 36^\circ$  (endplug EM calorimeter - central EM calorimeter). The separation between calorimeter arches at  $\theta = 90^\circ$  is 1 cm.

The interaction region is rather long at the Tevatron, about 70 cm full width at half maximum, leading to an effective smearing of the  $\theta$  boundaries in the calorimetry. A less pronounced smearing occurs in the  $\phi$ -direction for charged particles bent in the solenoid field. Characteristic sizes of the azimuthal boundary regions are indicated in Table 1.

The proportional tube chamber calorimeters provide not only the tower (cathode pad) signals described above, but also some wire pulse height information. Individual wires are not read out, but sums of wire signals, either from a section of a chamber or from a full chamber, are. The detailed information about longitudinal shower development coming from these wire sums can be very useful, both for diagnostic purposes, and for physics analysis, whenever particles are "isolated".

### 3. Electronics, triggering and readout

Crates of RABBIT (Redundant Analog Based Bus Information Transfer, see [8]) electronics are located on the detector on or near the respective calorimeters. These crates contain charge sensitive amplifiers [9], sample-and-hold capacitors and multiplexed 16 bit Analog to Digital Converters. "Scanners" located in the counting room are used to read out the ADC information and the channel addresses. Separate cables carry signals to the CDF trigger system [10].

A clock, synchronized to the accelerator radio frequency system, delivers timing signals to the electronics. The integration times currently used for the calorimeter signals are quite long, about  $0.6 \mu\text{s}$  for the phototube signals and about  $1.6 \mu\text{s}$  for the pad signals, some of which have large source capacitances (up to  $110 \text{ nF}$ ). Amplifier gain shifts of up to 15% are observed for the channels connected to the largest source capacitances. An on-card calibration system is used to measure the overall electronics gain, so that such effects can be corrected for in the data processing.

The rms electronics noise on an individual channel is equivalent to about  $0.03 \text{ GeV}$  of energy deposit in the tower, whereas full scale is set at about  $400 \text{ GeV}$ .

The readout of the phototubes on the scintillator hadron calorimeters includes the digitized value of the time at which the energy is deposited. This information is useful for rejection of events in which cosmic rays deposit large amounts of energy within the calorimeter signal integration time of a normal  $p\bar{p}$  event (overlap of cosmic ray and  $p\bar{p}$  event).

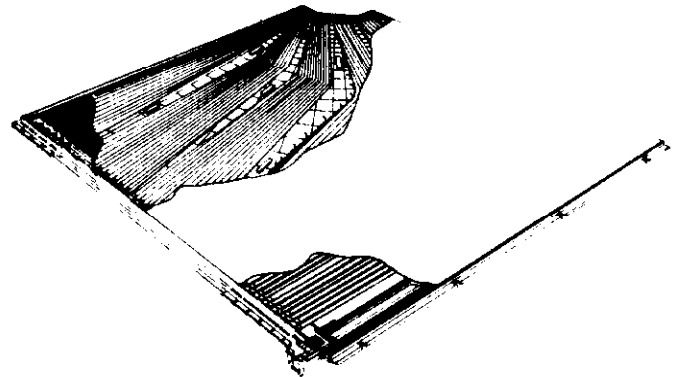


Fig. 5 Cutaway view of a proportional tube chamber in the forward EM calorimeter

## 4. Proportional tube chamber calorimeters

### 4.1 Description

The signal in the endplug and forward calorimeters is generated in sets of proportional tube chambers. These chambers cover  $90^\circ$  in  $\phi$  (a quadrant), except in the endplug hadron calorimeter, where structural supports are spaced at  $30^\circ$  intervals in  $\phi$ . The desired tower readout of these calorimeters is obtained by measuring the induced signals on cathode pads formed on the printed circuit boards of the chambers. The signals from corresponding pads at different depths are added together to form the total tower signal. A cutaway view of one of the chambers of the forward EM calorimeter [5], in which the cathode pads together with the readout lines that carry the signals from the pads to edge connectors on the side of the chamber, can be seen in Fig. 5. A chamber cross section is shown in Fig. 6. These chambers are made by gluing aluminum T's together to form U-channels, as shown in Fig. 6. The surface of the printed circuit board closes the U-channel.

The proportional tube chambers in the endplugs [3,4] are made from layers of individual conductive plastic tubes (extruded polystyrene mixed with carbon grains), which are glued to printed circuit boards. The tube resistivity (about  $100 \text{ k}\Omega$  per square) is high enough that the induced cathode signal will form on the pads of the printed circuit board beyond the

tube, yet low enough that the tube can serve as a conductor for the average current in the chamber.

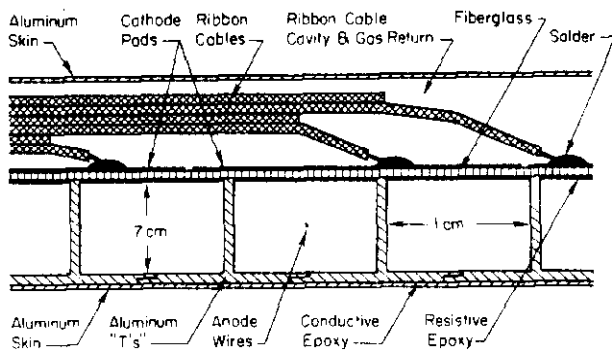


Fig. 6 Cross section of a chamber in the forward EM calorimeter

#### 4.2 Fabrication and quality control

The fabrication of, altogether, more than 1200 operating chambers with a total area of more than 1700 m<sup>2</sup> is clearly a major task which requires strict quality control and testing. The desire to make chambers with uniform gain leads to special requirements to quantities such as tube dimensions and straightness. Chamber performance tests have been carried out both during and after chamber construction. The part of the tests having to do with checking gain variations varies from system to system. In the forward calorimeters, where the control of tube size and straightness is easier, spot checks of chamber gains have been made with <sup>106</sup>Ru sources. For the endplug EM calorimeter, the wire gains of all chambers have been mapped with cosmic rays, and only chambers with rms variations of less than 5% have been retained. For the endplug hadron calorimeters, <sup>109</sup>Cd sources have been used to map both wire and pad gains of all chambers. This data shows that the wire gains are uniform to better than 5%, but that the pad gains (and the pad/wire ratios) are systematically about 20% higher at the edges of the chambers than in the middle for this system [11].

#### 4.3 Chamber operation and gain monitoring

The chambers of a given sector are all operated at the same high voltage. Changes in gain due to variations in pressure, temperature or gas composition are tracked by calibrated monitor tubes. Gain changes of 25% over a 24 hour period have been recorded when a pressure front moves through the laboratory, but different monitor tubes show the same gain change to within about 2%. Data from the test beams are still being analyzed to establish the connection between gain changes in the calorimeters and in the monitor tubes. Many subtle effects must be understood before the monitor tube gains can be used for accurate corrections. It appears likely that the ultimate precision with which calorimeter gain changes can be tracked with the monitor tubes will be about 2%, but this has not yet been achieved. We estimate that the current uncertainty in the absolute calibration of the proportional tube chamber calorimeters at a reference point (which relies on the transfer of monitor tube gain from the test beam to the experiment building) is about 10%.

The chamber gas is 50% argon, 50% ethane with a small admixture of alcohol. The chambers are operated in the proportional mode, with typical wire gains of about 10<sup>4</sup>, see Table 1. The ratio of the signal induced on the cathode pads to the anode wire signal is typically about 35% (it is system dependent).

#### 4.4 Test beam results

The sectors of the proportional tube chamber calorimeters each cover a rather large area of  $\eta$ - $\phi$  space, see for instance Fig. 4. There are few sector (chamber) boundaries, but many internal tower boundaries. The response (sum of tower signals) is basically constant across an internal boundary. There are, however, slow response variations across the full area of these calorimeters, primarily due to variations in the chamber pad gains. The response, for showers that are contained in the transverse direction, is within about  $\pm 10\%$  of the average response. A more precise knowledge of the response can be obtained by mapping in a test beam. An example of such mapping of the endplug EM calorimeter is shown in Fig. 7. The data obtained by measuring the response at the center of each tower can be used to describe the response everywhere to about 2% rms in this case.

The fractional area in which the response is reduced due to chamber boundaries in these calorimeters is very small, about 1%. Characteristic total widths of the boundary regions are indicated in Table 1.

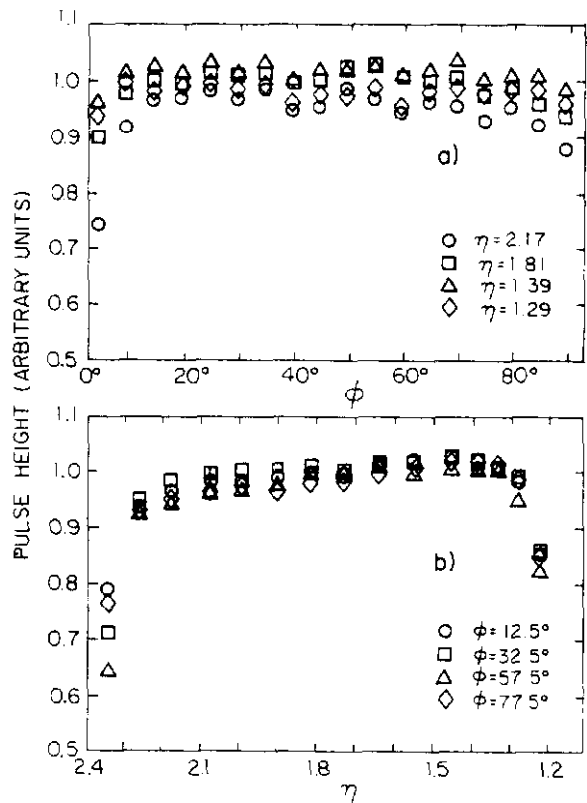


Fig. 7 Response of the endplug EM calorimeter to 100 GeV electrons for different impact points. The tower sum pulse height versus  $\phi$  is shown in a) for different  $\eta$ , while b) shows the variation in  $\eta$  for different  $\phi$ . The reduced response near the edges is due to energy leakage out of the calorimeter

Showers (both EM and hadronic) are typically spread over several towers in these calorimeters. One consequence of this is that shower positions can be determined with good accuracy, especially in case of high energy showers, as indicated in Table 1. This table also indicates energy resolutions at 50 GeV. The energy resolution varies with energy approximately as  $1/\sqrt{E}$ .

The energy dependence of the response of the EM calorimeters to electrons has been measured between 20 and 200 GeV, while the hadron calorimeter response to pions has been measured between 40 and 200 GeV. The measured response is linear with energy within about 5% in this energy range. Small deviations from linearity are observed in the EM calorimeters at the higher energies due to avalanche saturation and longitudinal energy leakage. The avalanche saturation effects in the EM calorimeters can be observed easily by raising the chamber high voltage 100 - 200 V above the values quoted in Table 1. Deviations from linearity are expected for the hadron calorimeters at low energy, but this energy region has not yet been measured.

#### 4.5 Definition of energy scales

Showers generated by high energy electrons are contained in the EM calorimeters, except for a small longitudinal leakage into the hadron calorimeters. For the showers generated by high energy charged pions, the situation is different. About 60% of these interact in the EM calorimeters, where they deposit on the average about 40% of their energy. The other 40% of the charged pions are minimum ionizing in the EM calorimeters, and therefore deposit all their energy in the hadron calorimeters (except for a small amount of leakage out the back). The hadron calorimeter pulse height of these pions is used to define the energy scale in the hadron calorimeters, while the energy scale in the EM calorimeters is defined by the response to energetic electrons. Pions of energy 200 GeV and electrons of energy 100 GeV are used in these definitions. The energy scale in the scintillator calorimeters is defined in the same manner, but with 50 GeV electrons and pions. The response of the combined endplug calorimetry to 200 GeV charged pions is shown in Figs. 8 and 9. The simplest algorithm for

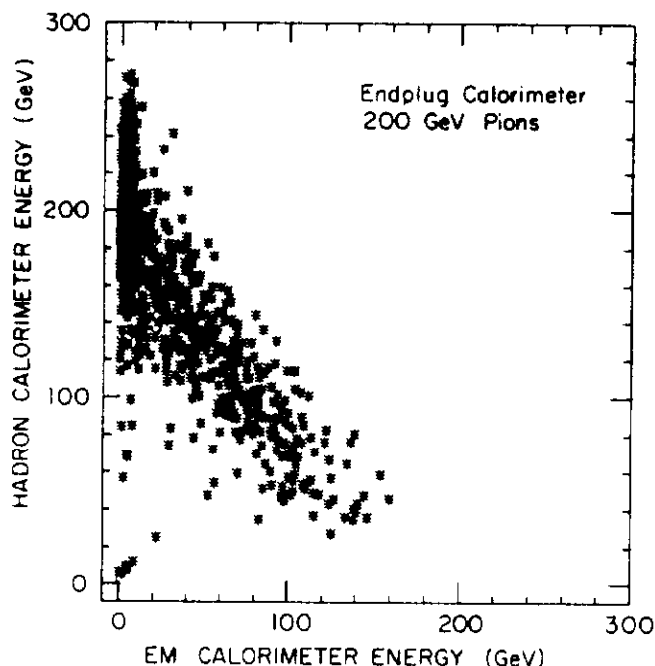


Fig. 8 Scatter plot of pulse heights in the endplug calorimeters for 200 GeV charged pions. The pulse height of 100 GeV electrons in the EM calorimeter is defined to be 100 GeV.

total energy, i.e. the sum of EM and hadronic energy, is used in this case. The average total pulse height for those pions that interact in the EM calorimeter is smaller than the average for those that are minimum ionizing in the EM calorimeter because the so-called pion/electron ratio (the pulse height ratio of equal energy pion and electron showers) is less than 1.0 in the EM calorimeter.

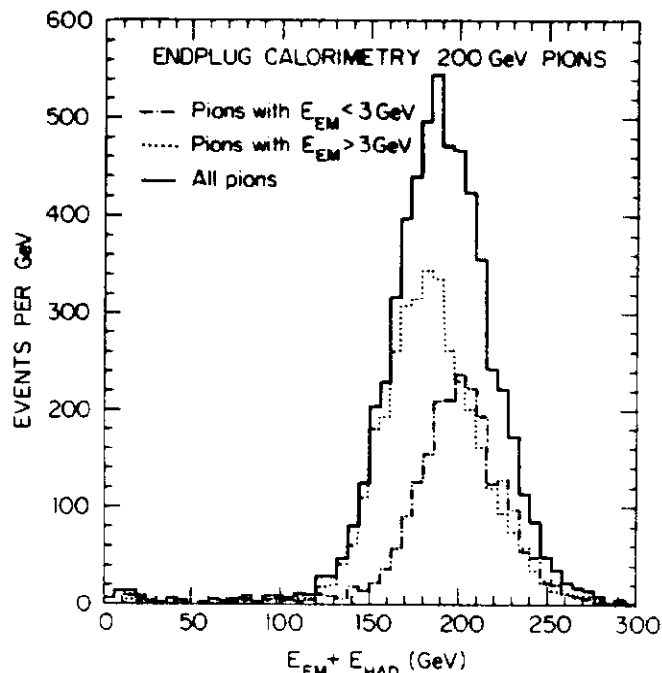


Fig. 9 Sum of EM and hadronic pulse heights for the data shown in Fig. 8. The distributions for all pions, and for those that leave more, respectively less than 3 GeV in the EM calorimeter, are shown separately.

## 5. Scintillator calorimeters

### 5.1 Description

A photograph of one of the 48 wedge modules taken during assembly is shown in Fig. 10. The ten towers of the EM calorimeter are located towards the bottom. The 0.5 cm thick pieces of polystyrene scintillator, doped with 1% butyl-PBD and 0.02% BDB (SCSN-38 from Kyowa Gas Chemical Ind. Co.) are individually wrapped in a double layer of vellum drawing paper. The inner edges are cut and polished, while the visible module surface is made by diamond fly cutting of the lead-scintillator stack. The stack is held together by the compressive force of a mechanical spring assembly, which occupies the space between the stack and the first steel plate of the hadron calorimeter. A proportional tube chamber is imbedded in the stack at a depth of about 5 radiation lengths. The size of the rectangular scintillator pieces at this depth is 46.2 cm in the  $\phi$ -direction (between wavelength shifters) and 24.1 cm in the direction of the beams.

Wavelength shifters on the two sides of a tower, consisting of 0.3 cm thick acrylic material, doped with Y7 wavelength shifter (also from Kyowa Gas Chemical Ind. Co.), are located in the 0.64 cm wide air gaps between the lead-scintillator stack and the 0.48 cm thick steel cover plate (not shown in the photograph). Light guides, about 1.5 m long and typically 2.0x2.5 cm<sup>2</sup> in cross section, carry the light from the glue joint with the wavelength shifter

to the "transition pieces" in front of the phototubes on the back of the module. For a fuller description, see [1].

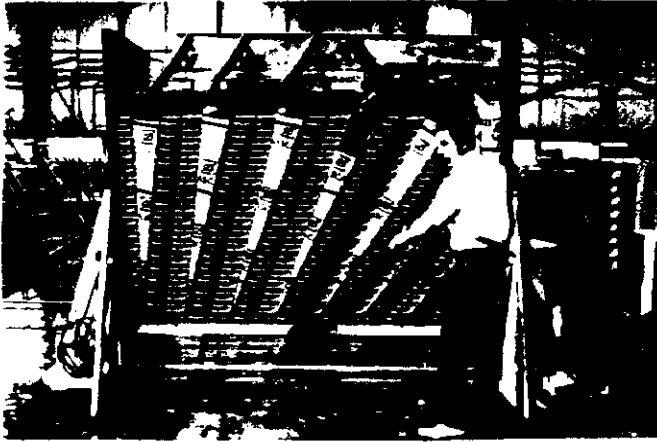


Fig. 10 Photograph of a 15 ton wedge module during assembly

The bulk of the module volume (Fig. 10) is taken by the eight towers of the central hadron calorimeter. The 1 cm thick pieces of acrylic scintillator, doped with 8% naphthalene, 1% butyl-PBD and 0.01% POPOP (from Polivar) are inserted in the 1.5 cm airgaps between the 2.5 cm thick steel plates. The four corners of the originally rectangular scintillator pieces are cut off to give room to the light guides of the EM calorimeter. The wavelength shifters are in this case  $0.5 \times 1.0$  cm<sup>2</sup> "fingers" of acrylic material (doped with Laser-dye #481) which form the boundaries in  $\theta$  between different towers. The scintillator-wavelength shifter combination is held together by an envelope of aluminum reflector bonded to a thin sheet of plastic. This "package" is in turn held in place by steel brackets welded to the calorimeter steel plates.

Individual finger light guides on each side of the module couple to the wavelength shifters via airgaps. These light guides are located in the 1.6 cm airgap between the steel cover plate and the steel plates of the hadron calorimeter.

The arrangement of scintillators, wavelength shifters and light guides in the endwall modules is very similar. These modules contain six towers, two of which overlap in angle with the last two towers of the central hadron calorimeter. For a more detailed description of these systems, see [2].

## 5.2 Fabrication and quality control

The scintillator calorimeters consist of 48 wedge modules (central calorimetry) and 48 endwall modules, each containing several towers. It is desirable to have all modules of a given type nearly identical in properties, so that common parameters can be used to describe them all. Strict quality control of components is again an ingredient in trying to achieve this. For scintillators, wavelength shifters and light guides, this amounts to controlling chemical composition, surface quality and thickness (and thereby attenuation length and light yield). The effects of remaining variations can be reduced by careful sorting of the materials. Quality control on the absorber plates is also required.

A special problem arises in the hadron calorimeters, because there are separate light guides

from each scintillator layer, see Fig. 10. The effect of this is that the light collected at the phototube of a given tower varies from layer to layer, by as much as a factor of two. The variation is part random, part systematic. A process of "layer equalization" has been performed on all modules to remove this variation. This process consists of the following steps: First, a frame with a movable <sup>137</sup>Cs source is mounted on the side of the module, and a light tight wooden box lowered over the module, so that the module is in complete darkness. A chart recorder is then used to measure the phototube d.c. current as the source is pulled at a constant speed along the side of the towers. Equalization of the response of all layers (to muons through the tower center) can be done by inserting a piece of black paper in the airgap between wavelength shifter and light guide to remove a fraction of the signal for layers with large signals. The size of each piece of paper can be calculated accurately from the measured response chart. The end result is that layers have been equalized to about 5% rms. The average reduction in total light output per tower due to this method of equalization is about 30%.

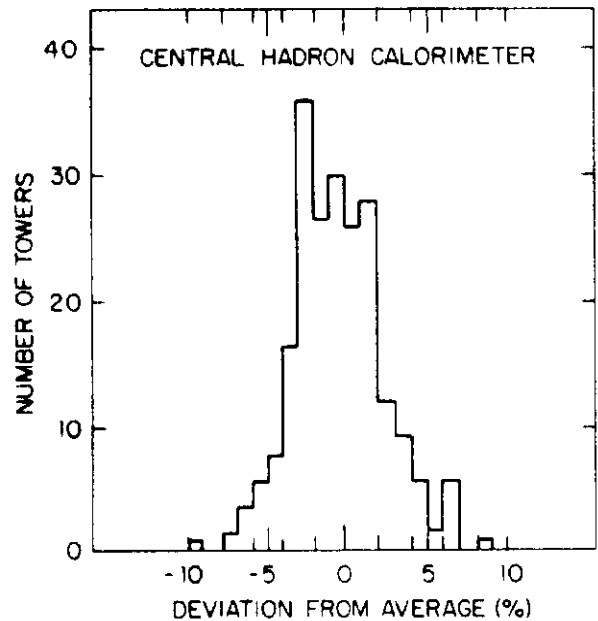


Fig. 11 Fractional response deviations from the average of each tower type in the central hadron calorimeter for 50 GeV charged pions after layer equalization with moving <sup>137</sup>Cs sources. The rms width is 2.5%.

A direct check of the resulting module similarity can be made by using the sources to set the phototube gains, and then measuring the response to pions in a test beam. The response deviation from the average for each tower type for pions hitting the tower center is shown in Fig. 11 for data from more than half the modules. The rms deviation is 2.5%.

The final check of wedge modules before transportation to the test beam consisted of a mapping of module response with cosmic ray muons, typically about 200 000 events per module. This data, together with test beam results, can be used to make a check of the module similarity of the central EM calorimeters. Fig. 12 shows the response ratio between 50 GeV electrons and cosmic ray muons at the center of a typical tower ( $\eta$  range from 0.26 to 0.38) for 46 wedges. The average ratio is 165, and the rms width

is 3.2%. This width represents an upper limit for the module dissimilarity, because both measurement errors in the determination of the muon peaks and phototube gain drifts between the two measurements widen the distribution.

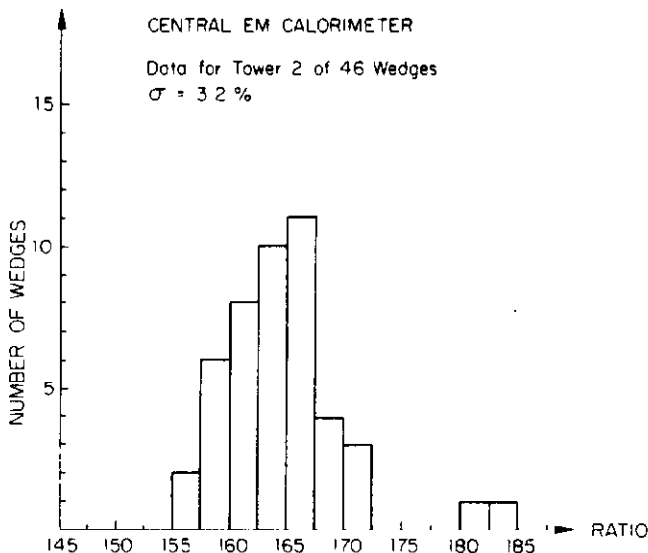


Fig. 12 Response ratio between 50 GeV electrons and cosmic ray muons at the center of one tower.

### 5.3 Scintillator calorimeter gain monitoring systems

Long term gain variations are monitored by a set of  $^{137}\text{Cs}$  sources, one per module, which can be moved through the module at a certain depth, thereby illuminating nearby scintillators in all the towers in turn by remote control. The source strength is 3 mCi for the wedges and 1.2 mCi for the endwall modules. The resulting d.c. currents, about 50 nA in the central EM calorimeter, 300 nA in the central hadron calorimeter and 120 nA in the endwall hadron calorimeter, are measured to an rms accuracy of 0.3-0.4%. An additional measure of module similarity for the central EM calorimeter, besides the measure quoted above, can be obtained by setting the phototube gains with these  $^{137}\text{Cs}$  sources, and then measuring the pulse height peaks for 50 GeV electrons at the tower centers for all modules. The resulting distribution is shown in Fig. 13. The full width at half maximum is about 8%.

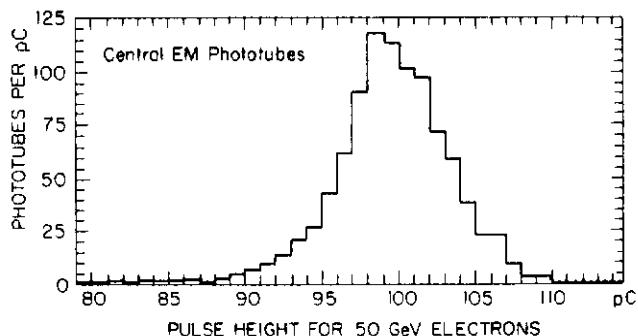


Fig. 13 Distribution of phototube pulse heights for all central EM calorimeters for 50 GeV electrons at the tower centers when the phototube gains have been set by the  $^{137}\text{Cs}$  sources

Short term gain changes are also monitored by light flasher systems. The central EM calorimeters employ two: a system using a Xe lamp, from which quartz fibers carry the light to the bottom of the wavelength shifter plates, and a LED (light emitting diode) system, in which quartz fibers carry the light to the transition piece in front of the phototube. The hadron calorimeters use a LASER to generate light signals for distribution via quartz fibers to the transition pieces in front of the phototubes.

The phototube gains are relatively low (see Table 1), and quite stable. Typical "light" yields are about 200 photoelectrons/GeV in the central EM calorimeter, about 40/GeV in the central hadron calorimeter, and about 24/GeV in the endwall hadron calorimeter (summed over phototubes in all cases). Photostatistics is therefore only a minor contribution to energy resolution in these systems.

### 5.4 Absolute calibration

A direct way to establish the absolute calibration is to measure the response to a test beam of known energy. This has been done for all wedge modules by directing 50 GeV electrons and charged pions at each tower center in turn, and thereafter also measuring the phototube response to the  $^{137}\text{Cs}$  sources. The absolute calibration at a later time can then be found simply by measuring again the d.c. current generated by the Cs sources, if one makes the assumption that the response ratio beam/source does not change with time. This assumption has been tested by repeated calibration of a few modules over a period of a few months, as shown in Fig. 14 for the central EM calorimeter. The result of this check is that the procedure has an accuracy of 0.6% rms and about 2% rms for the EM and hadron towers, respectively (pion peaks are fitted less accurately than electron peaks).

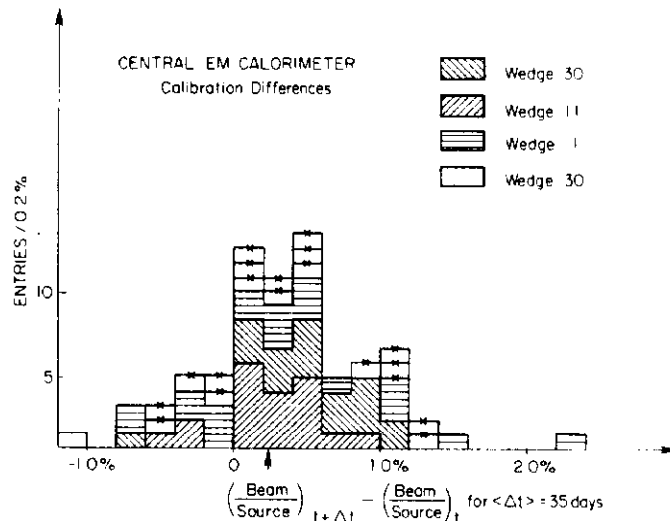


Fig. 14 Reproducibility of the calibration procedure for four wedges. The arrow indicates the expected shift of +0.22% in the beam/source ratio due to the 30 year half-life of  $^{137}\text{Cs}$ . The rms error is 0.6%.

A note about module orientation must be added at this point. All beam calibration was performed with modules in a horizontal position. The installation into the detector therefore included a module rotation. It is possible that such a rotation could cause slight motions of wavelength shifters and light

guides, which in turn might lead to small changes in the module calibration. We would expect that the  $^{137}\text{Cs}$  sources would track any changes of this type, but we currently have insufficient data to check this assertion at the 0.6% level.

The endwall modules were not available for test beam calibration because mapping of the solenoid field could only be done with these modules in place. The method used for absolute calibration in this case has been to calibrate the two spare modules in the beam, and to rely on the module similarity obtained by the layer equalization described in section 5.2 to estimate the calibration of the other modules. The result in Fig. 11 shows a variation of 2.5% (rms) between modules after equalization, so the estimated uncertainty in the knowledge of the absolute calibration of the endwall modules is of the order of 4% (rms).

All calibrations were done with a 6.4 cm thick plate of aluminum placed to simulate the effects of the solenoid coil.

### 5.5 Energy dependence and resolution

The energy dependence of the response of the scintillator calorimeters to electrons and pions has been measured between 10 and 150 GeV. The response is linear to within a couple of percent between 50 and 150 GeV, but there appear to be deviations from linearity at the lower energies for both EM and hadron calorimeters. Such deviations are not expected in the EM calorimeters (where they amount to 4% at 10 GeV). Whether errors in the measurement of low beam momenta or as yet unknown properties of the EM calorimeters are the cause of these deviations is not clear at present.

Energy and position resolutions at 50 GeV are indicated in Table 1. The energy resolution scales with energy approximately as  $1/\sqrt{E}$ .

### 5.6 Response maps

The response of the central EM calorimeter as a function of the impact point of 50 GeV electrons coming from the exact center of the interaction region is illustrated in Fig. 15. The impact points in this figure are limited to the area of a single tower, and the response is here taken as the sum of phototube pulse heights in this tower and the two adjacent ones in the same wedge. The coordinates used are  $x = R \tan \phi$  and  $z' = R \cot \theta - z_0$ , where  $R = 184.15$  cm is the radius at the imbedded proportional tube chamber. The map covers the full width of 24.1 cm in  $z'$ , but  $x$  is limited to the region  $-22.5 \text{ cm} < x < 22.5 \text{ cm}$ , thus excluding the boundary region in  $\phi$ , where the wavelength shifters are located (see section 5.7 for the response in this region). The normalized response, which is 1.00 in the center, varies between 0.92 and 1.08. Light attenuation in the scintillator is the cause of most of the response variation in  $x$ .  $P_0$  and  $P_1$ , the phototube pulse heights on the two sides of the tower, can be found from the approximate expressions  $P_0 + P_1 = E \cosh(x/\lambda_1)$  and  $P_0/P_1 = \exp(-2x/\lambda_2)$ . If a single exponential could express the effects of the light attenuation,  $\lambda_1$  would equal  $\lambda_2$ . The data indicates however that  $\lambda_1$  is  $44 \pm 5$  cm, while  $\lambda_2$  is  $88 \pm 8$  cm.

A 4% dip in the response at the  $\theta$  boundary between towers can be seen in Fig. 15. For collision points displaced along the beam axis, the calorimeter response will be smeared over a small region in  $z'$ , and this dip will therefore be less pronounced.

Mapping of five wedge modules with 50 GeV electrons indicates that a common response map (one for each of the ten towers in the modules), describes the module response to about 1.5% rms within the area  $-22.5 \text{ cm} < x < 22.5 \text{ cm}$ . The measurement of the shower position, which is used in conjunction with the response map, comes from the built-in proportional tube chamber. Within this area, the combined error from the absolute calibration (0.6% rms) and from the deviations from the average map (1.5%), are comparable to the energy resolution for 50 GeV electrons (2%). The total rms error is therefore of the order of 3% for 50 GeV electrons within this area.

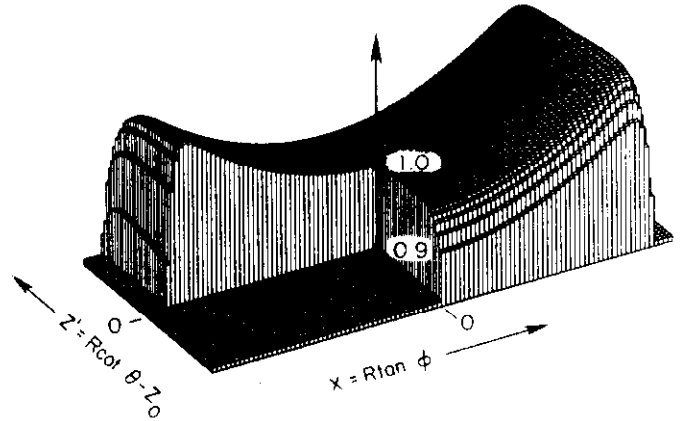


Fig. 15 Response map of the central EM calorimeter for 50 GeV electrons. The variation of the pulse height sum of the phototubes in the wedge is shown.

The response map of the central hadron calorimeter to 50 GeV pions is qualitatively similar to the EM calorimeter map discussed above. There is also a narrow response dip (of about 10%) at the  $\theta$  boundary for pions coming from the center of the interaction region. The variation in  $\phi$  of the pulse height sum (away from the  $\phi$ -boundary) is smaller than in the EM calorimeter because the relevant attenuation is now in the hadron calorimeter wavelength shifters (attenuation length 115 cm).

### 5.7 Boundary between wedges

A "hot spot" in the scintillator calorimeters was discovered in the region of the  $\phi$  boundary between modules when this region was first mapped in the test beam. By hot spot is meant that very large pulse heights are observed in phototubes of the hadron calorimeter when electrons (and to a lesser degree pions) are incident on this region. The signal is caused by generation of copious Cerenkov light in the light guides. Uranium bars, 3.5 cm wide and 3.0 cm (9 radiation lengths) deep (backed by a narrow proportional chamber) have been installed in the 6 cm open space between the coil and the front face of the wedge modules to attenuate EM showers, and thereby largely eliminate this undesired effect. The fraction of  $\phi$  covered by these Uranium bars is 8%. A schematic drawing of this boundary is shown in Fig. 16. The 3.5 cm width is sufficient to cover not only the normal 2.2 cm gap between lead-scintillator stacks shown in this figure, but also the 2.8 cm gap in the horizontal plane (at the middle of the arches), where a wedge shaped steel shim of maximum thickness 0.6 cm separates wedge modules, and the 2.5 cm gap in the vertical plane where 0.3 cm of air gap separates the calorimeter arches.

The region of this  $\phi$  boundary constitutes the largest nonuniformity in the response of the scintillator calorimeters. The calorimeter response across the  $\phi$ -boundary between wedges with the Uranium bars in place is not known, but test beam measurements with lead absorbers, which were used to arrive at the final design, are shown in Figs. 17 and 18 (for 8 radiation lengths of lead). The EM and hadronic energies in each wedge have been calculated separately using the algorithm  $E = \sqrt{PO \cdot P1}$  in this case.

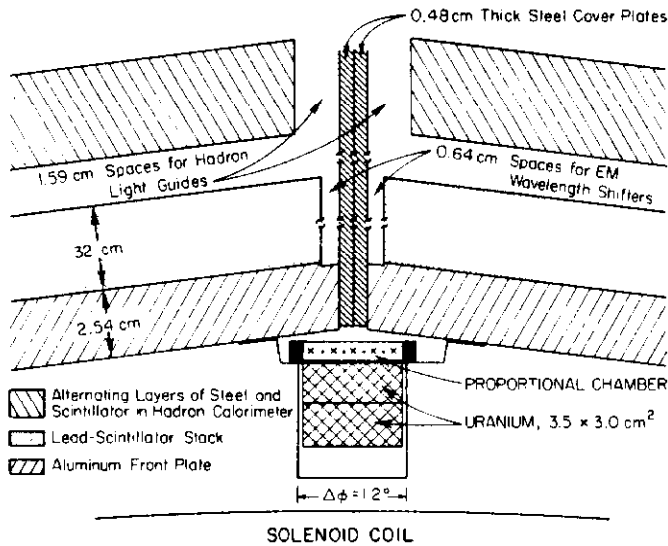


Fig. 16 Schematic drawing of the boundary region between two wedges

The chamber measures the energy of electrons incident on the lead bar with a resolution of about 25% (rms). When the chamber pulse height (suitably normalized) is added to the sum response of the EM and hadron calorimeters, one obtains a response to electrons which is approximately flat across the full  $\phi$ -range, but with an rms width in the boundary region of about 16%, not much larger than the typical hadron calorimeter energy resolution. The original hot spot has essentially disappeared because of the EM shower attenuation in the lead. Measurements with electrons of energies in the range 10-50 GeV show that all pulse heights are approximately proportional to the energy, so the 50 GeV electron data is representative of the overall effects.

The response to 50 GeV charged pions in the boundary region is smaller than elsewhere, and there is a probability of essentially zero response. The central tracking system will in many cases be able to measure the momenta of high energy charged particles pointing directly at a boundary region for which no corresponding signal is seen in the calorimeter.

### 5.8 Particle pulse height ratios

The pulse height of cosmic ray muons in the central EM calorimeter on a scale set by 50 GeV electrons is already reported in Fig. 12 as 50 GeV/165 or 0.30 GeV. The average energy loss of minimum ionizing particles in the lead-scintillator sandwich is 0.18 GeV, leading to a so-called electron/muon ratio of  $1/(0.3/0.18) = 0.6$ . The pion/muon ratio in the central hadron calorimeter can be determined in a similar way from a cosmic ray muon pulse height of 1.9 GeV and an average energy loss of minimum ionizing particles of 1.1 GeV, leading to pion/muon =  $1/(1.9/1.1) = 0.58$  (about 0.6 when corrected for the longitudinal energy leakage of 50 GeV pions).

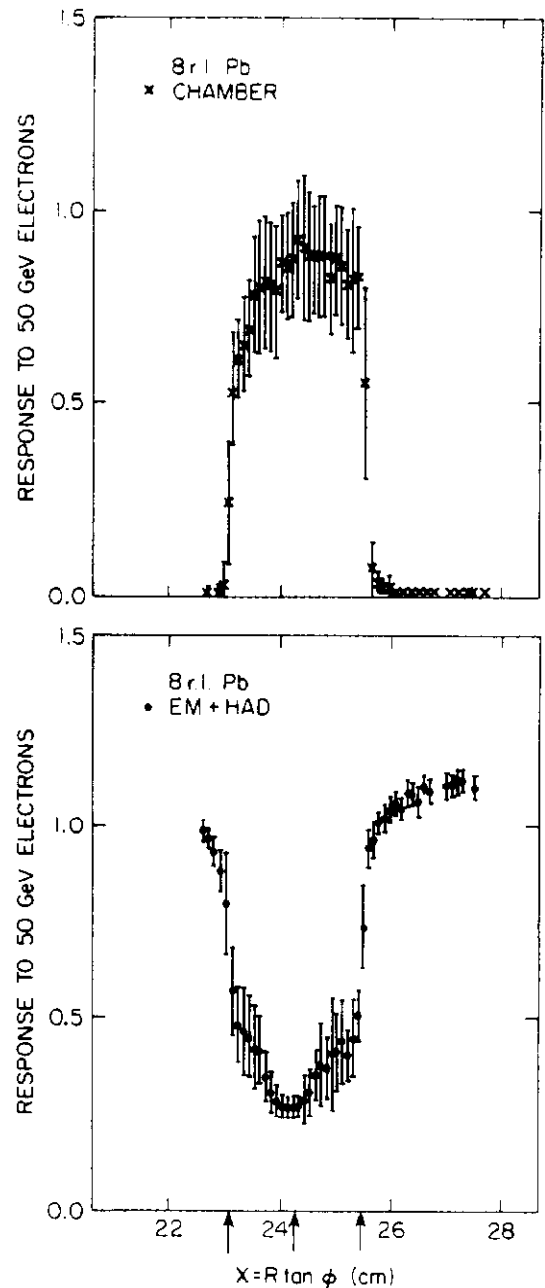


Fig. 17 Response of wedge modules and proportional chamber to 50 GeV electrons across the boundary region between wedges for  $\theta$  at the tower center. The center arrow indicates the center of the boundary region. The other arrows indicate the edges of the 2.5 cm wide lead bar.

### 6. Effects of the magnetic field

The accurate calibration systems of the scintillator calorimeters are very useful for studies of systematic effects in the calorimeters. An example of this is the measurement of the effects of the solenoid (fringe) field on the calorimeters. A small systematic increase in the signal from the  $^{137}\text{Cs}$  sources is found when the solenoid field is changed from 0 to 1.5 Tesla, even though no change in phototube gain (tracked with the light flasher systems) occurs [12]. The effect is caused by an increase in scintillator light yield in the presence of even small (order of 0.01 T) magnetic fields [13].

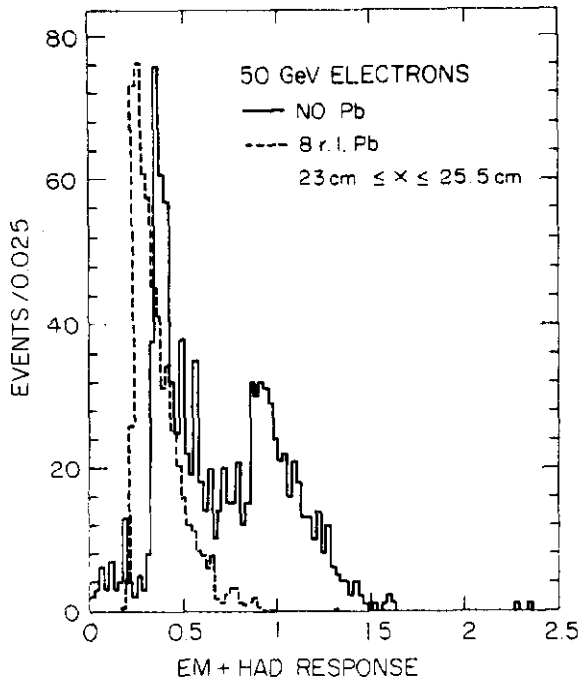


Fig. 18 Pulse height distributions for 50 GeV electrons in the wedge boundary region with and without the lead absorber in place. The response is calculated as  $\sqrt{PO \cdot PI}$  where PO and PI are the individual phototube pulse heights. The response is 1.0 at the tower center.

### 7. Conclusion

Extra modules, "identical" to the ones installed in the detector, have been fabricated so that test beam studies of calorimeter performance can continue. The immediate goal is to bring all these modules together in a single test beam, so that all boundary regions in the detector can be mapped. A number of other measurements, foremost among which is a detailed measurement of energy dependence of calorimeter response (especially at low energy), also remain to be done. Further questions will surely arise in the course of the analysis of data accumulated during the current physics run. We are optimistic, however, that the careful quality control exercised during the fabrication, combined with the quite extensive test beam measurements already carried out, will form a solid basis for analysis of calorimeter data.

### Acknowledgments

The author would like to thank J. Cooper, C. Haber, S. Hahn, T. Kamon, S. Mikamo, K. Yasuoka and B. Wicklund for providing figures for this paper.

### Appendix 1: CDF Collaboration

F. Abe<sup>a</sup>, D. Amidei<sup>c</sup>, G. Apollinarik, G. Ascoli<sup>g</sup>,  
M. Atac<sup>d</sup>, P. Auchincloss<sup>n</sup>, A. R. Baden<sup>f</sup>, V. Barnes<sup>l</sup>,  
E. Barsotti<sup>d</sup>, F. Bedeschnik, S. Belforte<sup>m</sup>,  
G. Bellottini<sup>k</sup>, J. Bensinger<sup>b</sup>, A. Beretvas<sup>n</sup>, P. Berged,  
S. Bertolucci<sup>e</sup>, S. Bhadra<sup>g</sup>, M. Binkley<sup>d</sup>, R. Blair<sup>a</sup>,  
C. Blocker<sup>f</sup>, G. Brandenburg<sup>l</sup>, A. Brenner<sup>d</sup>, D. Brown<sup>f</sup>,  
A. Byon<sup>l</sup>, M. Campbell<sup>c</sup>, R. Carey<sup>f</sup>, W. Carithers<sup>i</sup>,  
D. Carlsmith<sup>q</sup>, T. Carroll<sup>d</sup>, R. Cashmore<sup>l</sup>, F. Cervellik,  
K. Chadwick<sup>l</sup>, T. Chapin<sup>m</sup>, G. Chiarelli<sup>m</sup>, W. Chinowsky<sup>i</sup>,  
S. Cihangir<sup>o</sup>, D. Cline<sup>q</sup>, T. Collins<sup>d</sup>, D. Connor<sup>j</sup>,  
J. Cooper<sup>d</sup>, M. Cordellie<sup>e</sup>, M. Curatolo<sup>e</sup>, C. Day<sup>d</sup>,  
R. DelFabbro<sup>k</sup>, M. Dell'Orso<sup>k</sup>, L. DeMortier<sup>b</sup>,  
T. Devlin<sup>n</sup>, A. DiVirgili<sup>l</sup>, D. DiBitonto<sup>o</sup>, R. Diebold<sup>a</sup>,  
R. Downing<sup>g</sup>, T. Droeged, M. Eaton<sup>f</sup>, J. Elias<sup>d</sup>, R. Ely<sup>i</sup>,  
S. Errede<sup>g</sup>, B. Esposito<sup>e</sup>, A. Feldman<sup>f</sup>, B. Flaughern,  
E. Focardi<sup>k</sup>, G. W. Foster<sup>d</sup>, M. Franklin<sup>g</sup>, J. Freeman<sup>d</sup>,  
R. Frisch<sup>c</sup>, Y. Fukui<sup>h</sup>, I. Gaines<sup>d</sup>, A. Garfinkel<sup>l</sup>,  
P. Giannetti<sup>2</sup>, N. Giokaris<sup>m</sup>, P. Giromini<sup>e</sup>, L. Gladney<sup>j</sup>,  
K. Goulianos<sup>m</sup>, J. Grimsod, C. Grosso-Pilcher<sup>c</sup>,  
C. Haber<sup>i</sup>, S. Hahn<sup>j</sup>, R. Handler<sup>q</sup>, R. Harris<sup>i</sup>,  
J. Hauser<sup>c</sup>, Y. Hayashide<sup>p</sup>, R. Hollebeek<sup>l</sup>, L. Holloway<sup>g</sup>,  
P. Hun<sup>n</sup>, B. Hubbard<sup>i</sup>, P. Hurst<sup>g</sup>, J. Huth<sup>d</sup>, M. Ito<sup>p</sup>,  
J. Jaske<sup>q</sup>, H. Jensen<sup>d</sup>, U. Joshi<sup>n</sup>, R. Kadel<sup>d</sup>, T. Kamon<sup>p</sup>,  
S. Kanda<sup>p</sup>, I. Karliner<sup>g</sup>, H. Kautzky<sup>d</sup>, K. Kazlauskis<sup>n</sup>,  
E. Kearns<sup>f</sup>, R. Kephart<sup>d</sup>, P. Kesten<sup>b</sup>, H. Keutelian<sup>g</sup>,  
Y. Kikuchi<sup>p</sup>, S. Kim<sup>p</sup>, L. Kirsch<sup>b</sup>, S. Kobayashi<sup>3</sup>,  
K. Kondo<sup>p</sup>, U. Kruse<sup>g</sup>, S. Kuhlmann<sup>l</sup>, A. Laasänen<sup>l</sup>,  
W. Lia<sup>a</sup>, T. Liss<sup>c</sup>, N. Lockyer<sup>j</sup>, F. Marchetto<sup>o</sup>,  
M. Masuzawa<sup>p</sup>, P. McIntyre<sup>o</sup>, A. Menzione<sup>k</sup>, T. Meyer<sup>o</sup>,  
S. Mikamo<sup>h</sup>, M. Miller<sup>j</sup>, T. Mimashi<sup>p</sup>, S. Miozzie,  
S. Miscettie<sup>e</sup>, M. Mishina<sup>h</sup>, S. Miyashita<sup>p</sup>, H. Miyata<sup>p</sup>,  
S. Mori<sup>p</sup>, Y. Morita<sup>p</sup>, A. Murakami<sup>3</sup>, Y. Muraki<sup>4</sup>,  
C. Nelson<sup>d</sup>, C. Newman-Holmes<sup>d</sup>, L. Nodulmana,  
J. O'Meara<sup>d</sup>, G. Ott<sup>q</sup>, T. Ozaki<sup>p</sup>, S. Palanque<sup>d</sup>,  
R. Paolotti<sup>k</sup>, J. Patrick<sup>d</sup>, R. Perchonok<sup>d</sup>, T. Phillips<sup>f</sup>,  
H. Piekarz<sup>b</sup>, R. Plunkett<sup>m</sup>, L. Pondrom<sup>q</sup>, J. Proudfoot<sup>a</sup>,  
G. Punzik, D. Quarried, K. Ragani, G. Redlinger<sup>e</sup>,  
R. Rezmer<sup>a</sup>, J. Rhoades<sup>q</sup>, L. Ristorik, T. Rohaly<sup>j</sup>,  
A. Roodman<sup>c</sup>, H. Sanders<sup>c</sup>, A. Sansoni<sup>e</sup>, R. Sard<sup>g</sup>,  
V. Scarpine<sup>g</sup>, P. Schlabach<sup>g</sup>, P. Schoessow<sup>a</sup>, M. Schubl,  
R. Schwitters<sup>f</sup>, A. Scribano<sup>k</sup>, S. Segler<sup>d</sup>,  
M. Sekiguchi<sup>p</sup>, P. Sestini<sup>k</sup>, M. Shapiro<sup>f</sup>, M. Sheaff<sup>q</sup>,  
M. Shibata<sup>p</sup>, M. Shochet<sup>c</sup>, J. Siegrist<sup>i</sup>, V. Simaitis<sup>g</sup>,  
J. Simmons<sup>l</sup>, P. Sinervo<sup>j</sup>, M. Sivert<sup>5</sup>, J. Skarha<sup>q</sup>,  
D. A. Smith<sup>g</sup>, R. Snider<sup>c</sup>, L. Spencer<sup>b</sup>, R. St. Denis<sup>f</sup>,  
A. Stefanini<sup>k</sup>, Y. Takaiwa<sup>p</sup>, K. Takikawa<sup>p</sup>, S. Tarem<sup>b</sup>,  
D. Theriot<sup>d</sup>, J. Ting<sup>c</sup>, A. Tollestrup<sup>d</sup>, G. Tonelli<sup>k</sup>,  
Y. Tsay<sup>c</sup>, K. Turner<sup>d</sup>, F. Ukegawa<sup>p</sup>, D. Underwood<sup>a</sup>,  
C. van Ingend, R. VanBerg<sup>j</sup>, R. Vidal<sup>d</sup>, R. Wagner<sup>a</sup>,  
R. Wagner<sup>d</sup>, J. Walsh<sup>j</sup>, T. Watts<sup>n</sup>, R. Webb<sup>o</sup>,  
T. Westhusing<sup>g</sup>, S. White<sup>m</sup>, V. White<sup>d</sup>, A. Wicklund<sup>a</sup>,  
H. Williams<sup>j</sup>, T. Winch<sup>q</sup>, R. Yamada<sup>d</sup>, A. Yamashita<sup>p</sup>,  
K. Yasuoka<sup>p</sup>, G. Yeh<sup>d</sup>, J. Yohd, F. Zettik

Argonne National Laboratory<sup>a</sup>-Brandeis University<sup>b</sup>-  
University of Chicago<sup>c</sup>-Fermi National Accelerator  
Laboratory<sup>d</sup>-INFN, Frascati, Italy<sup>e</sup>-Harvard  
University<sup>f</sup>-University of Illinois<sup>g</sup>-KEK, Japan<sup>h</sup>-  
Lawrence Berkeley Laboratory<sup>i</sup>-University of  
Pennsylvania<sup>j</sup>-INFN, University of Pisa, Italy<sup>k</sup>-Purdue  
University<sup>l</sup>-Rockefeller University<sup>m</sup>-Rutgers  
University<sup>n</sup>-Texas A&M University<sup>o</sup>-University of  
Tsukuba, Japan<sup>p</sup>-University of Wisconsin<sup>q</sup> Collaboration

<sup>1</sup>Visitor from University of Oxford, England.

<sup>2</sup>Visitor from INFN Trieste, Italy.

<sup>3</sup>Visitor from Saga University, Japan.

<sup>4</sup>Visitor from ICRR, Tokyo University, Japan.

<sup>5</sup>Visitor from Haverford College, Haverford, PA.

**Table 1**  
**Summary of Calorimeter Properties**

	Central		Endwall	Endplug		Forward	
	EM	Hadron	Hadron	EM	Hadron	EM	Hadron
$ \eta $ -coverage	0-1.1	0-0.9	0.7-1.3	1.1-2.4	1.3-2.4	2.2-4.2	2.3-4.2
Tower size, $\Delta\eta \times \Delta\phi$	$\sim 0.1 \times 0.26$	$\sim 0.1 \times 0.26$	$\sim 0.1 \times 0.26$	$0.09 \times 0.09$	$0.09 \times 0.09$	$0.1 \times 0.09$	$0.1 \times 0.09$
Longitudinal samples in tower	1*	1	1	3	1	2	1
Active medium	polystyrene scintillator	acrylic scintillator	acrylic scintillator	Proportional tube chambers with cathode pad readout			
scintillator thickness or proportional tube size	0.5 cm	1.0 cm	1.0 cm	$0.7 \times 0.7 \text{ cm}^2$	$1.4 \times 0.8 \text{ cm}^2$	$1.0 \times 0.7 \text{ cm}^2$	$1.5 \times 1.0 \text{ cm}^2$
Number of layers	31	32	15	34	20	30	27
Absorber	Pb	Fe	Fe	Pb	Fe	94% Pb, 6% Sb	Fe
Absorber thickness	0.32cm	2.5cm	5.1cm	0.27cm	5.1cm	0.48cm	5.1cm
Typical phototube or wire high voltage	-1100V	-1500V	-1100V	+1700V	+2120V	+1900V	+2200V
Typical phototube or wire gain	$1.2 \times 10^5$	$6 \times 10^5$	$10^6$	$2 \times 10^3$	$2 \times 10^4$	$5 \times 10^3$	$10^4$
Typical tower signal	-4pC/GeV	-4pC/GeV	-4pC/GeV	+1.25pC/GeV	1.3pC/GeV	+2pC/GeV	+0.7pC/GeV
Energy resolution $\left(\frac{\sigma}{E}\right)$ at 50 GeV	2%	11%	14%	3%	20%	4.5%	23%
Typical position resolution at 50 GeV	$0.2 \times 0.2 \text{ cm}^{2*}$	$10 \times 5 \text{ cm}^2$	$10 \times 5 \text{ cm}^2$	$0.2 \times 0.2 \text{ cm}^2$	$2 \times 2 \text{ cm}^2$	$0.2 \times 0.2 \text{ cm}^2$	$3 \times 3 \text{ cm}^2$
Characteristic total width of azimuthal boundary region	3.5cm	4.1cm	3.8cm, 8.9cm alternating	0.9cm	0.8cm	0.7cm; 3.2cm**	1.3cm; 3.2cm**

\*An imbedded proportional tube chamber at shower maximum gives some additional information.

The quoted position resolution is measured with this chamber

\*\*The first number is for the vertical boundary, the second for the horizontal.

### References

- [1] Argonne National Laboratory, University of Tsukuba, Fermi National Accelerator Laboratory, KEK, University of Pennsylvania, Rutgers University; L. Balka et al., to be submitted to Nucl. Instr. and Meth.
- [2] INFN-Frascati, INFN-Pisa, Purdue University, Fermi National Accelerator Laboratory; S. Bertolucci et al., to be submitted to Nucl. Instr. and Meth.
- [3] KEK, Tsukuba University; Y. Fukui et al., to be submitted to Nucl. Instr. and Meth.; Y. Hayashide et al., submitted to Japanese Journal of Applied Physics (1987).
- [4] Lawrence Berkeley Laboratory; W. C. Carithers, W. Chinowsky, R. Elia, R.P. Ely, M.E.B. Franklin, C. Haber, R.M. Harris, B. Hubbard, N. Hunt, J. Ng and J.L. Siegrist, Proceedings of the Gas Sampling Calorimetry Workshop II, Fermilab (1985) 74.
- [5] Brandeis University, Harvard University; J. Bensinger et al., to be submitted to Nucl. Instr. and Meth.
- [6] Texas A&M University; J. Buchholz et al., to be submitted to Nucl. Instr. and Meth.
- [7] CDF Design Report, internal CDF report No. 111 (1981) unpublished; H. B. Jensen, IEEE Trans. Nucl. Sc., NS-33 No. 1 (1986) 40.
- [8] G. Drake, T.F. Droege, C.A. Nelson, K.J. Turner and T.K. Ohnska, IEEE Trans. Nucl. Sc., MS-33 No.1 (1986) 92.
- [9] G. Drake, T.F. Droege, S.R. Hahn, R. Van Berg, H.H. Williams, T.M. Liss, R.G. Wagner and S. Inaba, IEEE Trans. Nucl. Sc., MS-33 No. 1 (1986) 893
- [10] D. Amidei, M. Campbell, H. Frisch, C. Grosso-Pilcher, T. Liss, G. Redlinger, H. Sanders, M. Shochet, J. Ting, Y.D. Tsai, P. Gianetti, L. Ristori and M. Dell'Orso, IEEE Trans. Nucl. Sc., MS-33 No.1 (1986) 63.
- [11] W.C. Carithers, W. Chinowsky, R.P. Ely, M.E.B. Franklin, C. Haber, R. Harris, B. Hubbard and J.L. Siegrist, Proceedings of the Gas Sampling Calorimetry Workshop II, Fermilab (1985) 54.
- [12] S. Hahn, D. Connor, M. Miller and H. Williams, CDF internal note 443; M. Cordelli, M. Curatolo, B. Eposito, P. Giromini, S. Miscetti and A. Sansoni, CDF internal note 465.
- [13] C. Swenberg and N.E. Geacintov in: Organic Molecular Photochemistry (J. Birks, ed., J. Wiley and Sons, New York 1973) vol. 1; E. Jenicke, P. Liand, B. Vignon and R. Wilson, Nucl. Instr. and Meth. 126 (1975) 459.